

# Forecasting piston rod seal failure based on acoustic emission features in ARIMA model

Jørgen. F. Pedersen<sup>1</sup>, Rune Schlanbusch<sup>2</sup>, Vignesh. V. Shanbhag<sup>3</sup>

<sup>1,2,3</sup> Norwegian Research Centre, Energy & Technology Department, Jon Lilletuns Vei 9 H, 3. etg, 4879, Grimstad, Norway

*jorgen.fone.pedersen@gmail.com*  
*rusc@norceresearch.no*  
*vigs@norceresearch.no*

## ABSTRACT

Fluid leakage due to piston rod seal failure in hydraulic cylinders results in unscheduled maintenance, machine downtime and loss of productivity. Therefore, it is vital to understand the piston rod seal failure at initial stages. In literature, very few attempts have been made to implement forecasting techniques for piston rod seal failure in hydraulic cylinders using acoustic emission (AE) features. Therefore, in this study, we aim to forecast piston rod seal failure using AE features in the auto regressive integrated moving average (ARIMA) model. AE features like root mean square (RMS) and mean absolute percentage error (MAPE) were collected from run-to-failure (RTF) tests that were conducted on a hydraulic test rig. The hydraulic test rig replicates the piston rod movement and fluid leakage conditions similar to what is normally observed in hydraulic cylinders. To assess reliability of our study, two RTF tests were conducted at 15 mm/s and 25 mm/s rod speed each. The process of seal wear from unworn to worn state in the hydraulic test rig was accelerated by creating longitudinal scratches on the piston rod. An ARIMA model was developed based on the RMS features that were calculated from four RTF tests. The ARIMA model can forecast the RMS values ahead in time as long as the original series does not experience any large shifts in variance or deviates heavily from the normal increasing trend. The ARIMA model provided good accuracy in forecasting the seal failure in at least two of four RTF tests that were conducted. The ARIMA model that was fitted with 15 pre-samples was used to forecast 10 out of sequence samples, and it showed a maximum moving absolute percentage error (MAPE value) of 28.99 % and a minimum of 4.950 %. The forecasting technique based on ARIMA model and AE features proposed in this study lays a strong basis to be used in industries to schedule the seal change in hydraulic cylinders.

## KEYWORDS:

Hydraulic cylinder, Piston rod seal, Root mean square, Variable speed condition, Auto-regressive integrated moving average, Acoustic emission.

## 1. INTRODUCTION

A hydraulic cylinder is a linear actuator which is widely used in material handling applications in oil and gas (O&G), maritime, mining and construction industries. Based on the material handling requirements: load handling and speed condition of hydraulic cylinders frequently change. In most applications, customized large hydraulic cylinders are used by the industries where all the internal components are also custom-made (See ref. (“Large Hydraulic Cylinder”). Any abrupt failure of a hydraulic cylinder component can cause machine downtime, affect productivity, and increase maintenance cost as most of the components in large hydraulic cylinders are custom made and require several weeks time of planning, manufacturing, and assembling the part back into the hydraulic cylinder. Seal wear in hydraulic cylinders can be because of particle contaminants present in fluid or seal ageing and can cause instability during operation (X. Zhao et al. 2015; Shanbhag et al. 2021b). Therefore, it is important to continuously monitor and forecast the health of crucial components such as the piston rod seals in the hydraulic cylinders.

In recent years, acoustic emission sensors have been widely used to monitor fluid leakage due to seal wear in hydraulic cylinders. Acoustic emission (AE) sensors are preferred by researchers because of their high frequency range (0.5-2.5 MHz) which make them suitable to use in noisy or harsh environments, and they be used to simultaneously monitor the health of multiple components in hydraulic cylinders. For example, (Chen et al. 2007), monitored the health of seals in water hydraulic cylinders using time domain (root mean square (RMS) and count) and frequency domain (power spectral density (PSD)) features. Fluid leakage (< 1.0 L/min) due to seal wear could be monitored using energy-based

Jørgen. F. Pedersen et al. This is an open-access article distributed under the terms of the Creative Commons Attribution 3.0 United States License, which permits unrestricted use, distribution, and reproduction in any medium, provided the original author and source are credited.

features (e.g., RMS). A correlation could be observed between fluid leakage rate and RMS. In the PSD plot, the fluid leakage was dominant in the frequency range of 50-300 kHz with a peak at 120 kHz. In the other work of (Petersen et al. 2005), monitored the health of the piston in a water hydraulic system using AE and wavelet analysis. RMS, PSD, and RMS of wavelet co-efficient were used to detect cracks in the piston rod. Using time domain feature RMS, it was possible to identify crack conditions in the piston rod. Compared to PSD, RMS calculated from wavelet co-efficient showed better separability between no-cracks and cracks in the piston rod. (Shanbhag et al. 2020), monitored the health of piston rod seals (unworn, semi-worn and worn conditions) on a customized hydraulic test rig using AE time-domain and frequency-domain features at different pressure conditions. It was observed that, the mean-frequency feature showed a good repeatability with sensitivity in identifying different seal wear conditions in the hydraulic test rig. In another work, (Shanbhag et al. 2021a) monitored the health of multiple components (piston rod seals and bearing strips) in the hydraulic test rig using AE time-domain and frequency-domain features to the bandpass filtered AE signal. Here, the unworn and worn bearing strips were monitored when unworn, semi-worn and worn seals were used in the test rig. The median-frequency features showed good repeatability in identifying piston rod seal wear and bearing wear conditions at different pressure and fluid leakage conditions. Also, mean-frequency and median-frequency showed good sensitivity in identifying fluid leakage due to piston rod seal wear during RTF tests (17 hours). (Zhang et al. 2021) monitored no leakage and different severities of fluid leakage (small, medium, and severe) in a hydraulic cylinder using an AE sensor. To classify the severity of fluid leakage, an optimization deep belief network (DBN) combined with the Complete Ensemble Empirical Model Decomposition with Adaptive Noise (CEEMDAN) was used and classification accuracy up to 93 % was achieved. (Pedersen et al. 2021), performed run-to-failure tests at different pressure and speed conditions on a hydraulic test rig to understand the AE features that can be evaluated to determine fluid leakage initiation. RMS features were proposed as potential condition monitoring indicators to understand fluid leakage initiation. The scaling factors based on sensor location and speed were applied to the sampled RMS features to estimate the fluid leakage threshold. From the literature, in the work performed using AE to monitor seal wear, most of the work is focused on condition monitoring (diagnostics) and very limited attempts in forecasting the deterioration and seal failure (prognostics).

The auto-regressive integrated moving average (ARIMA) model is a time series forecasting technique that is widely used in different applications such as disaster management, business forecasting, and machine prognostics. The ARIMA model can be used to understand the change in signal features with spatial heterogeneity over time (Li et al. 2021). In

literature, the ARIMA technique has been applied using AE features to predict a) energy change in gas-liquid two-phase flow (N. Zhao et al. 2021), b) coal and gas outburst (Li et al. 2021). As the ARIMA technique has successfully been used with the AE features for forecasting the process change or failure of components, the ARIMA technique in this research is used with AE features for forecasting the seal degradation. In this paper, the AE data from our previous experimental study conducted by (Pedersen et al. 2021) is used for forecasting analysis.

## 2. METHODOLOGY

### 2.1. Hydraulic test rig and process parameters

In this study, experiments were conducted on a test rig installed in an upright position (Figure 1) and was designed to replicate the fluid leakage conditions of a hydraulic cylinder. The test rig consists of three major items: a) test arrangement (electromechanical cylinder with pressure chamber), b) hydraulic system providing hydraulic power, c) control box which controls and monitors the test rig. The control box is connected to a laptop using an Ethernet cable and the test rig is controlled using the Bosch Rexroth software “IndraworksDs- 14.24.6”. A hydraulic power unit (HPU) supplies pressure to the pressure chamber in the test rig, which can be controlled using a pressure valve. The pressure chamber is connected to an electromechanical cylinder. The electromechanical cylinder consists of servomotor, spindle, and piston rod. The electromechanical cylinder uses a spindle and nut to convert rotational motion to translational motion. The servomotor drives the spindle, and the driven nut is connected to the piston rod. The piston rod in the test rig reciprocates through the pressure chamber that is made pressure tight using a typical rod-sealing concept. During the experiments, the chamber is pressurized while circulating medium (fluid) through the chamber to absorb heat and any debris caused by the seal wear.

In the test rig, five types of seals were used: a) wiper seal, b) excluder seal, c) secondary rod seal, d) primary rod low friction seal, and e) rod bearing ring. In this study, only the secondary rod seal and primary rod low friction seal were replaced with new seals during every test as the wear of these seals results in fluid leakage. Replacement took place during every test as the wear of these seals used to results in fluid leakage. Seal failure was defined when fluid leakage was observed from the leakage port in test rig. Typically, the seal life used in hydraulic cylinders in industry is for several years. However, in this study, the seal wear was accelerated by inducing scratches on the piston rod using a hard metal tip scribing tool. The process parameters used for the experiments are listed in Table 1.

Fluid in test rig	Water glycol
Rod material	Chromium-molybdenum steel (+QT) with 20µm HCr coating

Primary and secondary seal material	Polytetrafluoroethylene (PTFE)
Pressure	15 bar
Piston rod speed	15 mm/s (Test 2 & 3) and 25 mm/s (Test 1 & 4)
Number of tests	4
Test run time	Until fluid leakage observed
Stroke length	75 mm (Test 1 & 4); 150 mm (Test 2 & 3)

Table 1. Experimental details.

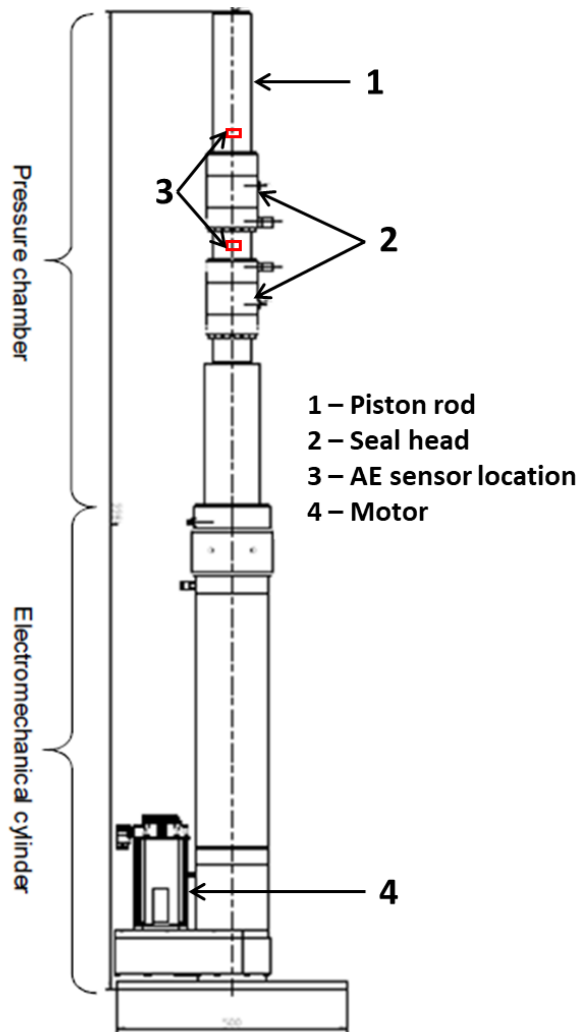


Figure 1. Schematic view of test rig.

### 2.2. Acoustic emission and signal processing

The AE sensor was mounted at two locations on the test rig: a) directly on the piston rod and, b) on the section of the cylinder below the seal head (see red squares indicating the positions in Figure 1). These two locations were selected as the measured AE signal energy was higher compared to other locations on the test rig. A mid-frequency range AE sensor with a frequency operating range of 50-400 kHz and resonant

frequency of 150 kHz was used in the study. The AE sensor was securely clamped on the test rig using an adhesive bond together with adhesive tape. The AE sensor was connected to a pre-amplifier and the pre-amplifier was further connected to an AE data acquisition system. The data acquisition system was connected to a laptop through a USB port. The AE data acquisition was performed using the Vallen AE suite software.

For all the experiments, the AE data acquisition was performed in continuous mode at a sampling rate of 1 MS/s and pre-amplifier gain of 40 dB. Due to the high sampling rate and the large size of the AE files, the AE data acquisition was limited to 90 seconds (five piston rod strokes) and data acquisition was performed at 15 minutes interval until the fluid leakage was observed. The AE signal was further analyzed using the MATLAB software. The AE signal of the extension and retraction strokes was observed to be similar (Figure 2). Therefore, only the AE signal from the extension stroke was used for forecasting analysis.

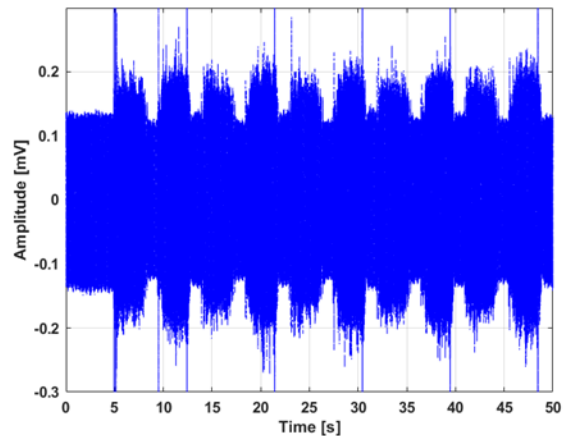


Figure 2. Raw AE signal recorded from test rig (Pedersen et al. 2021)

For every RTF test, a new piston rod seal was used in the seal head. Therefore, every test required the removal of the AE sensor from the test rig. To ensure, that the AE sensor clamping is consistent for every test, the Hsu-Nielsen pencil lead break test (See ref (“Acoustic Emission (AE): Hsu-Nielsen Source”)) was performed before the start of each test. The pencil lead break test was performed by breaking a 0.5 mm diameter pencil lead on the test rig surface near the mounted sensor. The amplitude of the AE burst response and magnitude of AE frequency response was calculated and compared during every test to ensure consistency of the AE sensor clamping on the test rig.

### 2.3. Auto-regressive moving average model

The ARIMA model is used in prediction of different types of time series data, e.g. financial or disaster prediction, as it can make the difference calculation in non-stationary time series data to form a stable series (Li et al. 2021). The ARIMA

model: a) auto-regressive (AR), b) integrated part (I), c) moving average part (MA). The ARIMA model is represented as ARIMA (p, d, q). Where, p is the order of the regressive model, d is the degree of difference, and q is the order of moving average model. The p, d, and q are used to make the model data as fit as possible. As per (Lee et al. 2011), the ARIMA model can be represented as a combination of past observations and past errors. The auto-regressive (AR) model uses past values in the time series to predict the future values in a time series. The AR model of order p, can be represented as:

$$x_n = \phi_1 x_{n-1} + \phi_2 x_{n-2} + \dots + \phi_p x_{n-p} + \omega_n \quad (1)$$

where in Eq. (1),  $x_n$  is the stationary time series,  $\omega_n$  is Gaussian white noise series, and  $\phi_1, \phi_2, \dots, \phi_p$  are the AR constants determined by an optimisation algorithm such as ordinary least squares (Shumway et al. 2017).

The moving average (MA) model uses its previous errors to make a prediction of future values. Here, the errors are the difference between the predicted value and the observed value. The MA model of order q, can be represented as:

$$x_n = \omega_n + \theta_1 \omega_{n-1} + \theta_2 \omega_{n-2} + \dots + \theta_q \omega_{n-q} \quad (2)$$

where in Eq. (2),  $\omega_n$  is white noise, and  $\theta_1, \theta_2, \dots, \theta_q$  are parameters (Shumway et al. 2017).

The integrated part (I) in the ARIMA model, means that the original timeseries are transformed from  $x_n$  to  $z_n$  via Eq. (3),

$$z_n = x_{n+1} - x_n \quad (3)$$

to make it stationary. The order of the integration parameter d is the order of difference performed on the time series.

### 2.3.1. Modelling of the condition monitoring data

In this study, the RTF test data was fitted using the ARIMA model. The Box-Jenkins model was used to select ARIMA (p, d, q) parameters and to validate the model fit. Each data set from the RTF test was used to fit in the ARIMA model to the most suitable condition monitoring data. To replicate a real-life condition, where the future data is unknown, only a portion of the initial samples were applied to fit the ARIMA model. The initial samples are labelled as pre-sample data. For creating the ARIMA model, fifteen samples from each RTF test were used as the pre-sample data. To test the accuracy of the developed ARIMA model, the next ten samples were used to forecast and to calculate the residual error. Based on the residual error, the root mean square error (RMSE) and the mean absolute percentage error (MAPE) was calculated as shown in Eq. (4). and Eq. (5).

$$MAPE = \frac{1}{n} \sum_{i=1}^n \left| \frac{x_i - \hat{x}}{x_i} \right| \times 100 \quad (4)$$

$$RMSE = \sqrt{\frac{\sum_{i=1}^n (x_i - \hat{x})^2}{n}} \quad (5)$$

where,  $x_i$  is the true value,  $\hat{x}$  is the forecasted value, and n is the number of forecasted samples.

The auto-correlation function (ACF) and partial auto-correlation function (PACF) were used to graphically represent the relationship of a data point in a timeseries to data points from previous timesteps. These previous timesteps are called lags. Thus, a lag of one represents one timestep prior to the current timestep. Autocorrelation is then the calculated correlation between the current value and the values at the lags in a timeseries (Salvi 2019). Table 2 was used as a reference to determine preliminary values of the p and q parameters. The MATLAB in-built function was used to estimate the ARIMA (p, d, q) model from the pre-sample data. After estimating the model fitting parameters, the goodness of fit was validated by inferring the residuals from the fitted model. The selected ARIMA (p, d, q) model was then used to forecast the datapoints of the holdout data. The residuals were calculated from the known values of the holdout data and subtracting it from the forecasted values, and then the MAPE and RMSE were calculated. To compare the error values, the pre-sample data and holdout data were standardized by normalizing the values in the range of zero to one. To increase accuracy of the forecasted timeseries, a Monte Carlo simulation was applied to the forecasting timeseries. The Monte Carlo simulation used one thousand forecasting iterations with the pre-sample data as the input data. The mean of the forecasted predictor values was then used as the forecasted values.

	AR(p)	MA(q)	ARMA(p,q)
ACF	Tails off	Cuts off after lag q	Tails off
PACF	Cuts off after lag p	Tails off	Tails off

Table 2. Behavior of ACF and PACF for ARMA models (Shumway et al. 2017).

## 3. RESULTS AND DISCUSSION

### 3.1. Pencil lead break test

Figure 3 a)-b) represent the AE time domain signal of the background noise and from the pencil lead break test respectively. The AE signal of background noise was recorded while the HPU was circulating hydraulic fluid in the pressure chamber. By comparing Figure 3 a)-b), the maximum amplitude of the AE signal from the pencil lead break test is at least hundred times higher compared to the HPU background noise. Figure 3 c)-d), represent the AE frequency response calculated using Welch’s method. The frequency responses show that, the AE frequency peaks are dominant in the frequency range of 65-190 kHz. The maximum magnitude of the frequency response of the background noise is about one thousand times smaller than for the pencil break test. As the effect of ground noise on the AE signal is minimal, bandpass filtering techniques were not applied for the AE signal recorded during the RTF tests.

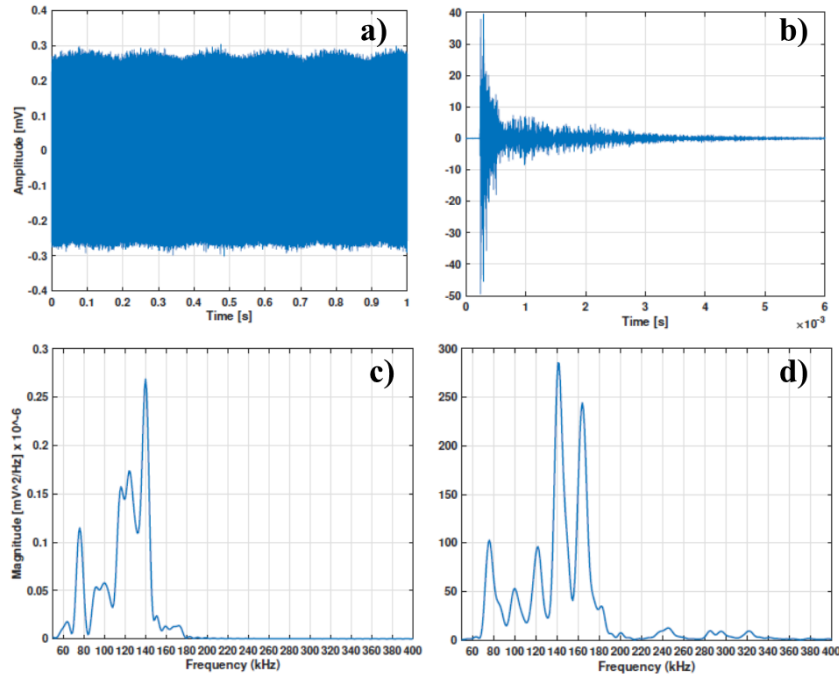


Figure 3. AE signal from a) Background noise, b) Pencil lead break test; Frequency response calculated from AE signal c) Background noise, d) Pencil lead break test.

### 3.2. ARIMA model using the RMS feature

From the RTF tests conducted a comparison of the time and frequency domain features were conducted, and it was observed that the RMS feature was the most suited for use as condition monitoring indicators to identify wear of piston rod seals (Pedersen et al. 2021). Therefore, in this study, the RMS feature was used to develop the ARIMA model. Figure 4-a) shows a plot of the RMS response for all four RTF tests. The signal was subtracted by the first sample to remove the bias and for easier comparison of the results. The increase in trend is similar for RTF tests 2 and 3 (tests conducted at 15 mm/s speed). For RTF 1 and 4, the trend shows a large difference (tests conducted at 25 mm/s speed). The drop in RMS feature in RTF 4, is mainly because the test was stopped at evening and restarted next day (in most industries hydraulic cylinders are used intermittently, not continuously). This has been done to observe the changes in signal response when the test rig was stopped. Tests 1 and 2 were run continuously, tests 3 and 4 were stopped in the night. In test 3, the next day system was switched on and kept running to allow system to be stabilized. Whereas in test 4 the next day, the system was switched on and data was recorded immediately to see the difference in behaviour of AE features with that of AE features from test 3. Furthermore, the transient response for the first three hours in RTF test 1 does not conform well to forecasting by the ARIMA model due to its initial decreasing trend. This is mainly because test rig pressure, and temperature require some time to stabilize. Therefore, for remaining tests, test rig was started only when test rig pressure and temperature were stabilized. To be able to do a better prediction on the RTF test

1 dataset, the transient response was removed. Figure 4-b) shows the responses for all RTF tests with the transient decreasing trend of RTF test 1 removed. As seen from Figure 4, the RMS feature trend is not stationary due to the increasing trend. To meet the stationary criteria of the ARIMA model, the RMS feature was differentiated. For RTF tests 1 and 3, a first order differentiation was applied, and for RTFs test 2 and 4, a second order differentiation was applied. Therefore, the differencing term ‘d’ in the ARIMA (p, d, q) was thus set as one for RTF tests 1 and 3, and two for RTF tests 2 and 4.

To identify the preliminary values of the AR (p) order, p, and MA (q) order, q, the ACF and PACF were plotted using the RMS features that were differentiated. Figure 5 shows the ACF and PACF plots for all differentiated data of the RTF tests. To find the initial parameters of the p, d, and q parameters for the ARIMA model, the guide in Table 2 was used to interpret the ACF and PACF plots. In Table 2, by “tailing off” it indicates the gradually decreasing correlation values, while the “cutting off” indicates the sudden large drop in correlation value. It can be seen in the PACF plot for RTF test 1 in Figure 5-e) that the PACF cuts off after the second lag. The ACF plot in Figure 5-a) does not show any lag above the threshold line, but it can be said to cut off after the first lag, even though the first lag is not very significant. An ARIMA (2,1,1) was thus suggested for the RMS signal from RTF test 1. For RTF test 2, both the ACF and the PACF plots in Figure 5-b) and Figure 5-f) show only one significant lag. However, the ACF plot can be seen to tail off while the PACF

plot cuts off at lag one. An ARIMA (1,2,0) model was thus suggested for the RMS signal from RTF test 2. The ACF plot for RTF test 3, in Figure 5, show very low correlation throughout the series, and only the second lag appears to show any correlation before it cuts off. The same can be seen for the PACF plot in Figure 5-g). Thus, to best model the RMS series for RTF test 3, an ARIMA (2,1,2) was suggested. Finally, for RTF test 4, the ACF plot in Figure 5-d) shows that it cuts off at the first lag. Similarly, the PACF plot in Figure 5-h) shows the same, but here the second lag can be seen to be more significant. Even though the second lag does not reach above the threshold line, it should still be utilized

in the model. An ARIMA (2,2,1) was thus suggested for the RMS series for RTF test 4.

The quantile-quantile (QQ) plots for the residuals of the fitted model on the pre-sample data is shown in Figure 6. It can be seen that all fitted models are reasonably normally distributed, except for the possible outliers as seen for the last quantile of RTF tests 1 and 4 in Figure 6-a) and Figure 6-d). The ACF and PACF plots of the residuals of the fitted models are represented in Figure 7. The models fitted to the RMS series for all RTF tests show a low correlation of the residuals both for the ACF and PACF. This indicates that the selected p, d, and q parameters provide good model fits to the data.

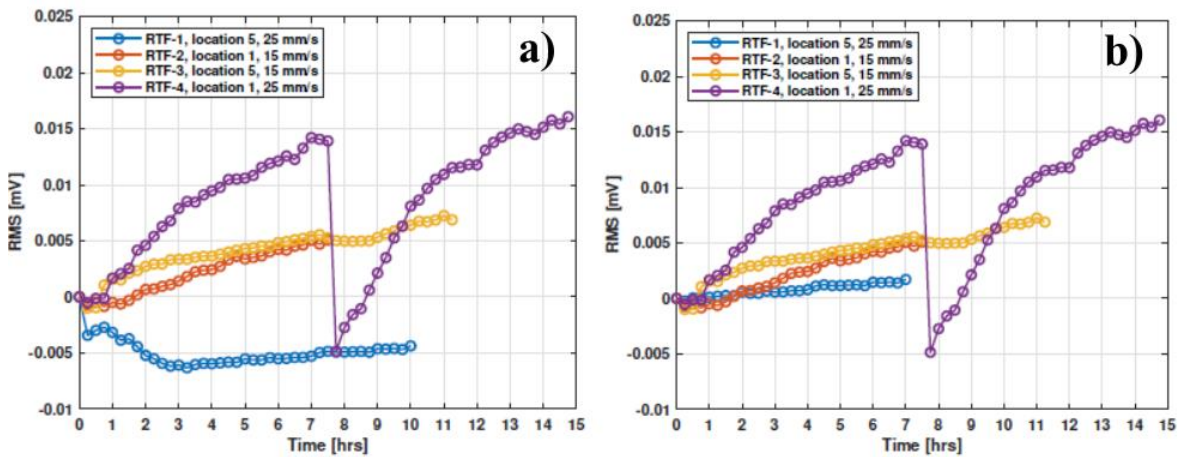


Figure 4. a) With transient from RTF test 1, b) Transient removed from RTF test 1.

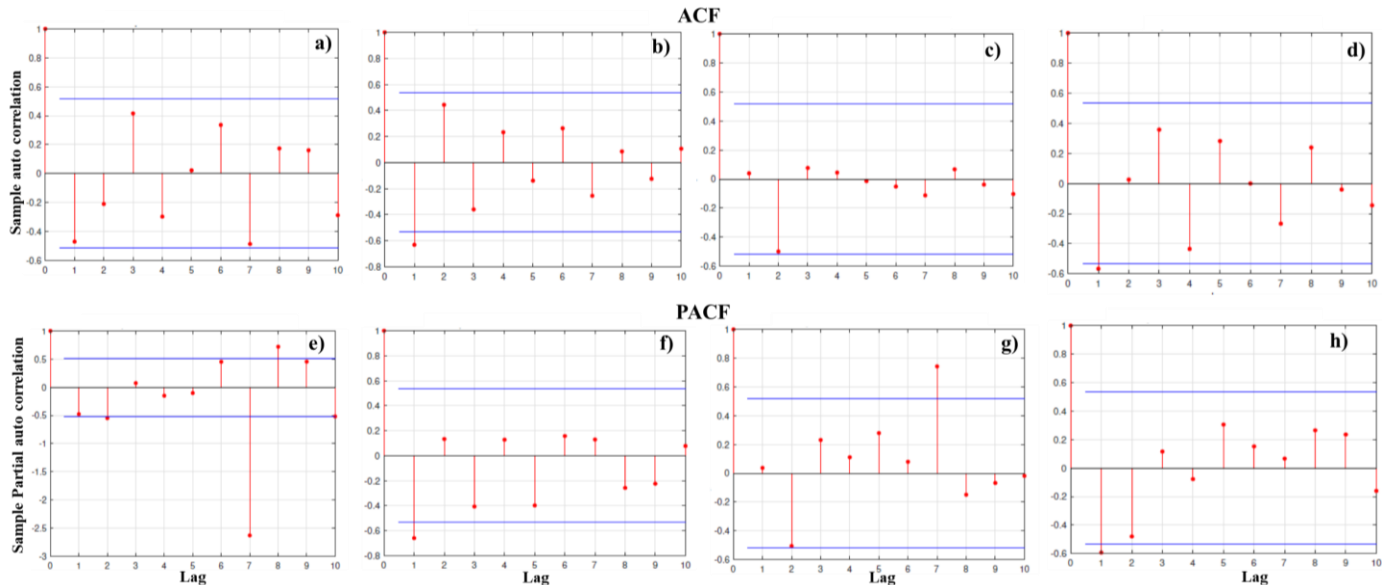


Figure 5. ACF and PACF for the differentiated RMS series of all RTF datasets, showing first 10 lags. a)-d) ACF, RMS signals from RTF 1-4, e)-f) PACF, RMS signals from RTF 1-4.

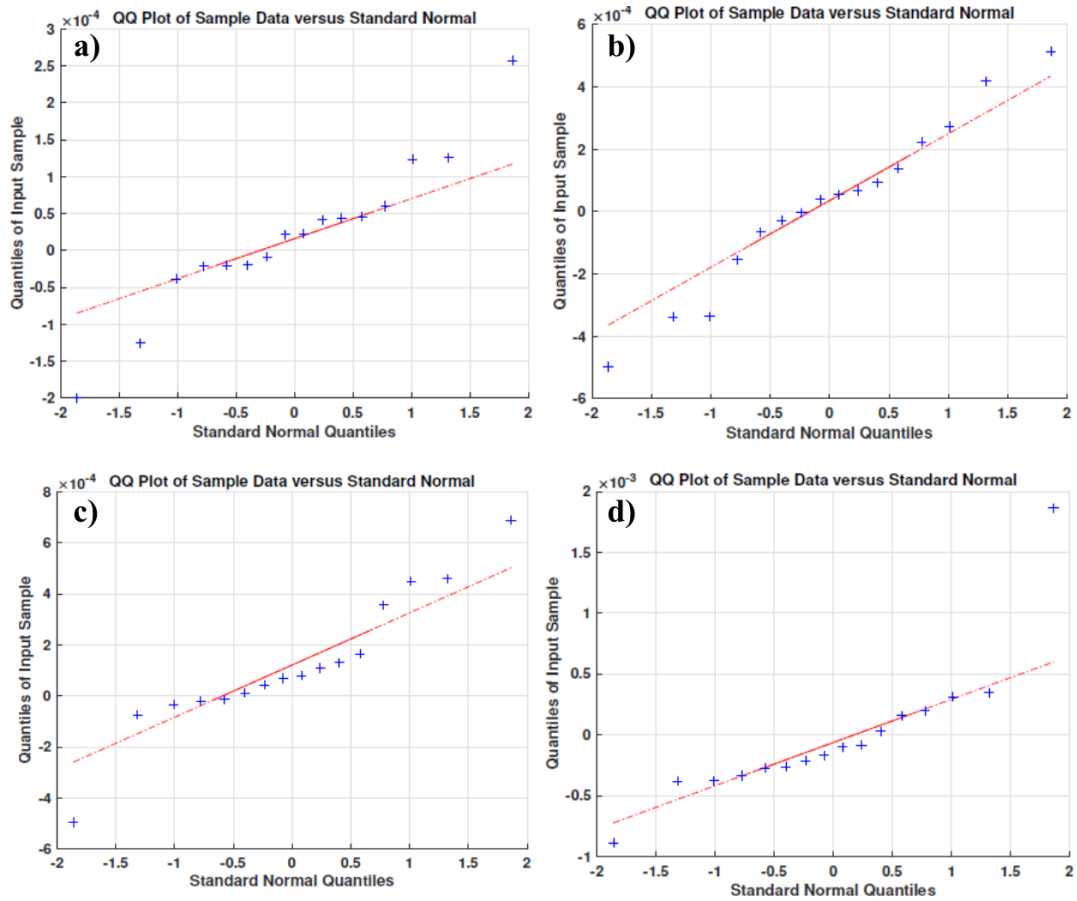


Figure 6. QQ plots for fitted ARIMA models to the RMS series of RTF tests 1 to 4: a) for ARIMA (2, 1, 1) model on RTF test 1, b) for ARIMA (1, 2, 0) model on RTF test 2, c) for ARIMA (2, 1, 2) model on RTF test 3, d) ARIMA (2, 2, 1) model on RTF test 4.

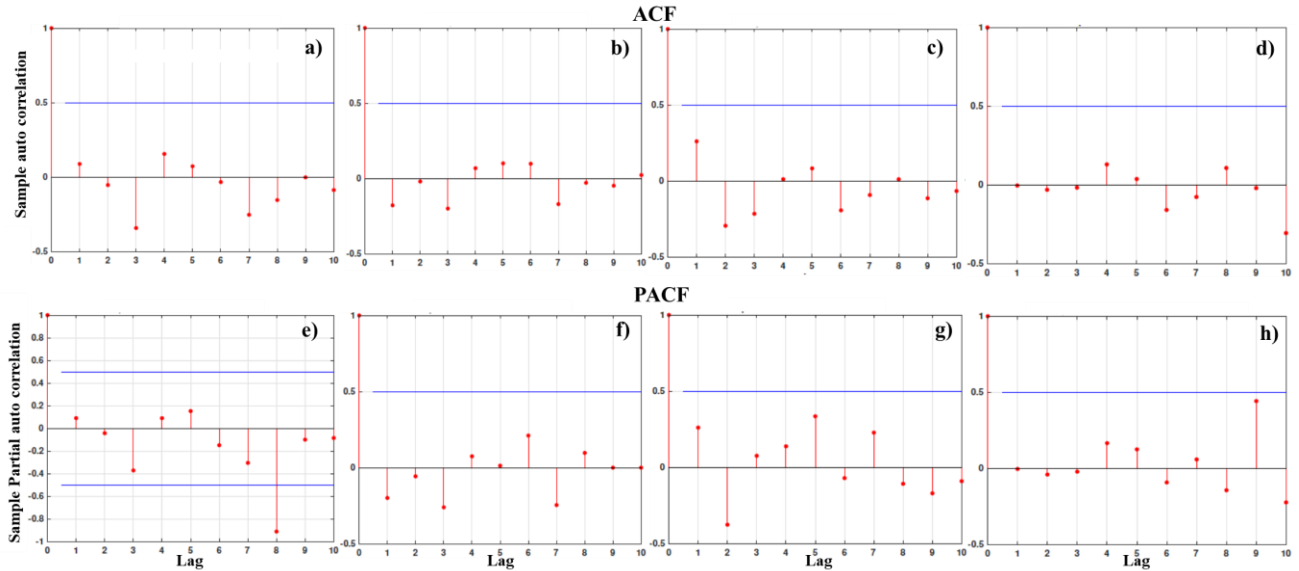


Figure 7. ACF and PACF for the residuals of the fitted ARIMA models on the pre-sample data. ACF for residuals of a) ARIMA (2, 1, 1) model on RTF test 1, b) ARIMA (1, 2, 0) model on RTF test 2, c) ARIMA (2, 1, 2) model on RTF test 3, d) ARIMA (2, 2, 1) model on RTF test 4. PACF for residuals of e) ARIMA (2, 1, 1) model on RTF test 1, f) ARIMA (1, 2, 0) model on RTF test 2, g) ARIMA (2, 1, 2) model on RTF test 3, h) ARIMA (2, 2, 1) model on RTF test 4.

### 3.3. Forecasting using the ARIMA model

Table 3 represents the best fitted ARIMA model parameters with the RMSE and MAPE values for the ten samples out of sequence forecasts. Figure 8 represents the forecasting of the RTF test data using the ARIMA model with the 95th percentile of the forecasts from the Monte-Carlo simulation. For all RTF tests, the forecasting plot can be seen to follow the increasing trend of the true data. Comparing the forecasting trend among the data from the RTF tests 1-4, for the RTF tests 1 and 2, see Figure 8 a)-b), the accuracy is less compared to RTF tests 3 and 4. The low accuracy of the forecast trend in RTF test 1 is mainly due to the large variance shift in the original dataset seen at around 4 hours, see Figure 4-a)). For the RTF test 2, the low accuracy for the ARIMA model is attributed to the low correlation of sequence that was

seen in the related ACF and PACF. For RTF tests 3 and 4, the ARIMA models displays good accuracy for the forecasted values, see Figure 8 c)-d) despite the low correlation of sequence also for these timeseries. The better accuracy of the model for RTF 3 and 4, can also be attributed to a favorable time of forecasting in the series.

RTF	AR (p)	I(d)	MA(q)	RMSE (mV)	MAPE (%)
1	2	1	1	0.187	20.26
2	1	2	0	0.326	28.99
3	2	1	2	0.053	4.95
4	2	2	1	0.104	8.88

Table 3. ARIMA (p, d, q) model parameters with the respective RMSE and MAPE error.

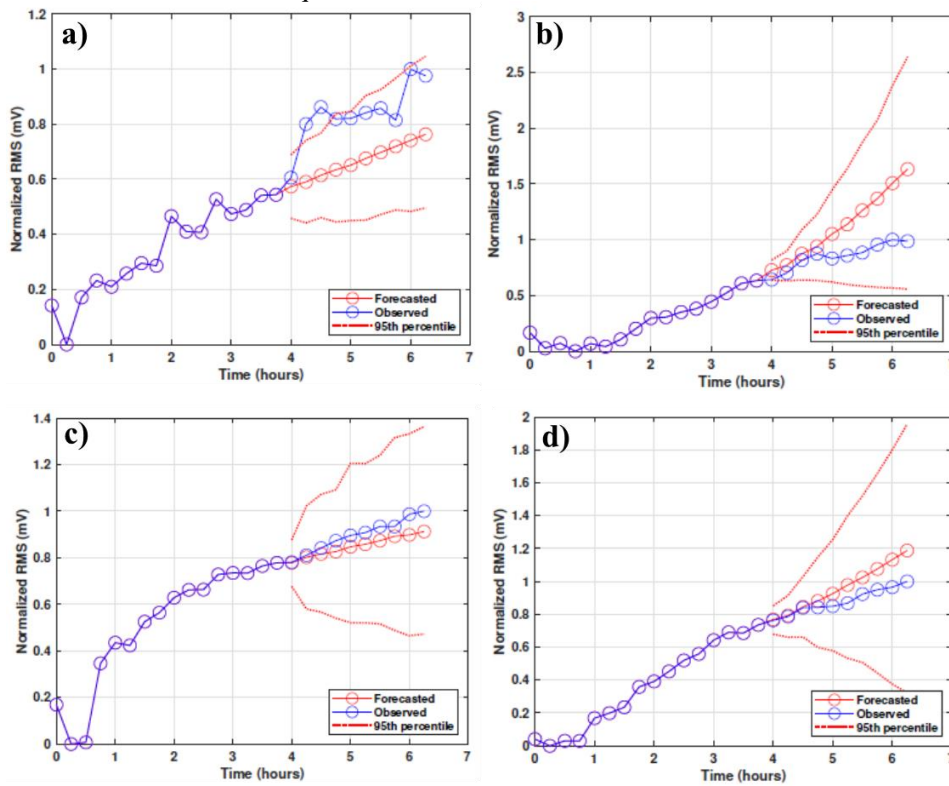


Figure 8. Forecasted data on 10 sample forecasts for RMS series of all RTF tests. a) For ARIMA (2,1,1) model on RTF test 1, b) For ARIMA (1,2,0) model on RTF test 2, c) For ARIMA (2,1,2) model on RTF test 3, d) For ARIMA (2,2,1) model on RTF test 4.

### 4. SUMMARY

In this study, the AE-RMS feature from four RTF tests was used to forecast the seal degradation process in a hydraulic test rig using an ARIMA model. The ARIMA model was able to forecast the RMS values ahead in time as long as the original RMS trend did not experience any large shifts in variance or deviates from the normal increasing trend, as is expected from this method. The ARIMA model showed that it can perform with good accuracy for forecasting in at least two of four RTF tests that were conducted. The ARIMA model that was fitted with fifteen pre-samples, was used to

forecast ten out of sequence samples, and it showed a maximum moving absolute percentage error (MAPE) a maximum of 28.99 % and a minimum of 4.950 %.

Based on the work conducted in this study, the authors conclude that further work is required with other modelling approaches like different variants of neural network for forecasting the seal failure, to improve the prediction when there are large shifts in variance that was seen in the RMS trend. Also, additional RTF tests need to be conducted with similar conditions to assess the repeatability of the forecasting technique.

## Acknowledgement

The research presented in this paper has received funding from the Norwegian Research Council, SFI Offshore Mechatronics, project number 2378.

## REFERENCES

- Chen, P., P.S.K. Chua, and G.H. Lim. 2007. "A Study of Hydraulic Seal Integrity." *Mechanical Systems and Signal Processing* 21 (2): 1115–26. <https://doi.org/10.1016/j.ymsp.2005.09.002>.
- "Large-Hydraulic-Cylinder-Brochure.Pdf." n.d. Accessed March 28, 2022. [https://dc-corp.resource.bosch.com/media/general\\_use/products/industrial\\_hydraulics\\_1/cylinders\\_1/Large-Hydraulic-Cylinder-Brochure.pdf](https://dc-corp.resource.bosch.com/media/general_use/products/industrial_hydraulics_1/cylinders_1/Large-Hydraulic-Cylinder-Brochure.pdf).
- Lee, Yi-Shian, and Lee-Ing Tong. 2011. "Forecasting Time Series Using a Methodology Based on Autoregressive Integrated Moving Average and Genetic Programming." *Knowledge-Based Systems* 24 (1): 66–72. <https://doi.org/10.1016/j.knosys.2010.07.006>.
- Li, Bing, Enyuan Wang, Zheng Shang, Xiaofei Liu, Zhonghui Li, Baolin Li, Hao Wang, Yue Niu, and Yue Song. 2021. "Optimize the Early Warning Time of Coal and Gas Outburst by Multi-Source Information Fusion Method during the Tunneling Process." *Process Safety and Environmental Protection* 149 (May): 839–49. <https://doi.org/10.1016/j.psep.2021.03.029>.
- "NDT Encyclopedia - Acoustic Emission (AE): Hsu-Nielsen Source." n.d. Accessed March 28, 2022. <https://www.ndt.net/article/az/ae/hsunielensource.htm>.
- Pedersen, Jørgen F., Rune Schlanbusch, Thomas J. J. Meyer, Leo W. Caspers, and Vignesh V. Shanbhag. 2021. "Acoustic Emission-Based Condition Monitoring and Remaining Useful Life Prediction of Hydraulic Cylinder Rod Seals." *Sensors* 21 (18): 6012. <https://doi.org/10.3390/s21186012>.
- Petersen, Dr, Re Link, P Chen, Psk Chua, and Gh Lim. 2005. "An Experimental Study of Monitoring Internal Leakage in Water Hydraulic Cylinders Using Acoustic Emission." *Journal of Testing and Evaluation* 33 (6): 12534. <https://doi.org/10.1520/JTE12534>.
- Salvi, Jayesh. 2019. "Significance of ACF and PACF Plots In Time Series Analysis." Medium. March 27, 2019. <https://towardsdatascience.com/significance-of-acf-and-pacf-plots-in-time-series-analysis-2fa11a5d10a8>.
- Shanbhag, Vignesh V., Thomas J. J. Meyer, Leo W. Caspers, and Rune Schlanbusch. 2020. "Condition Monitoring of Hydraulic Cylinder Seals Using Acoustic Emissions." *The International Journal of Advanced Manufacturing Technology* 109 (5–6): 1727–39. <https://doi.org/10.1007/s00170-020-05738-4>.
- Shanbhag, Vignesh V., Thomas J. J. Meyer, Leo W. Caspers, and Rune Schlanbusch. 2021a. "Defining Acoustic Emission-Based Condition Monitoring Indicators for Monitoring Piston Rod Seal and Bearing Wear in Hydraulic Cylinders." *The International Journal of Advanced Manufacturing Technology* 115 (9–10): 2729–46. <https://doi.org/10.1007/s00170-021-07340-8>.
- Shanbhag, Vignesh V., Thomas J. J. Meyer, Leo W. Caspers, and Rune Schlanbusch. 2021b. "Failure Monitoring and Predictive Maintenance of Hydraulic Cylinder—State-of-the-Art Review." *IEEE/ASME Transactions on Mechatronics* 26 (6): 3087–3103. <https://doi.org/10.1109/TMECH.2021.3053173>.
- Shumway, Robert H., and David S. Stoffer. 2017. *Time Series Analysis and Its Applications: With R Examples*. Springer Texts in Statistics. Cham: Springer International Publishing. <https://doi.org/10.1007/978-3-319-52452-8>.
- Zhang, Peng, and Xinyuan Chen. 2021. "Internal Leakage Diagnosis of a Hydraulic Cylinder Based on Optimization DBN Using the CEEMDAN Technique." Edited by Li Qing. *Shock and Vibration* 2021 (March): 1–10. <https://doi.org/10.1155/2021/8856835>.
- Zhao, Ning, Chaofan Li, Huijun Jia, Fan Wang, Zhiyue Zhao, Lide Fang, and Xiaoting Li. 2021. "Acoustic Emission-Based Flow Noise Detection and Mechanism Analysis for Gas-Liquid Two-Phase Flow." *Measurement* 179 (July): 109480. <https://doi.org/10.1016/j.measurement.2021.109480>.
- Zhao, Xiuxu, Shuanshuan Zhang, Chuanli Zhou, Zhemin Hu, Rui Li, and Jihai Jiang. 2015. "Experimental Study of Hydraulic Cylinder Leakage and Fault Feature Extraction Based on Wavelet Packet Analysis." *Computers & Fluids* 106 (January): 33–40. <https://doi.org/10.1016/j.compfluid.2014.09.034>.